Journal of Clinical Neuroscience 145 (2026) 111851

Contents lists available at ScienceDirect

Journal of Clinical Neuroscience

journal homepage: www.journals.elsevier.com/journal-of-clinical-neuroscience

# A novel application of radiomics for the evaluation of transient wall shear stress on the surface of cerebral aneurysms

Alexandra Lauric, Adel M. Malek *

*Cerebrovascular Hemodynamics Laboratory, Department of Neurosurgery, Tufts Medical Center and Tufts University School of Medicine, Boston, MA 02111, USA*

ARTICLE INFO

*Keywords:*
Intracranial aneurysms
Computational fluid dynamics
Wall shear stress
Radiomics
Ruptured status

ABSTRACT

*Background:* Intracranial aneurysm evaluation based on computational fluid dynamic (CFD) wall shear stress (WSS) analysis remains an active and evolving research field. We propose a novel application of radiomics for transient CFD, focusing on texture and pattern evaluation of aneurysmal WSS, beyond conventional distribution analysis.

*Methods:* Catheter 3D rotational angiographic volumes were available for 75 aneurysms (33 ruptured). Transient CFD simulations were performed on aneurysmal models across the cardiac cycle, exporting WSS distributions at 25 consecutive time steps. 3D WSS distributions were mapped to 2D by projection to unit sphere, followed by normalization and logarithmic transformation for analysis at extrema. The resulting 2D spatial WSS images over time formed 3D DICOM volumes for radiomics analysis. Uni- and multivariate analysis was used to evaluate radiomics features for rupture status discriminant performance.

*Results:* Compared to unruptured, ruptured aneurysms show increased complexity and heterogeneity in the spatial and temporal domains (higher DifferenceEntropy, JointAverage, JointEntropy), with distinct areas of low and high WSS-derived intensity (lower InverseDifference, higher SumAverage). Ruptured aneurysms showed significantly less uniformity of pattern both in size (higher SizeZoneNonUniformity) and intensity (higher GrayLevelNonUniformity). Multivariate analysis for rupture status discrimination resulted in an area under the curve (AUC) value of 0.81 (sensitivity 0.82, specificity 0.72).

*Conclusion:* Radiomics analysis of transient WSS resulted in strong rupture status discrimination. This novel approach extends the use of radiomics beyond angiographic analysis, enables evaluation of WSS evolution over the entire cardiac cycle, provides insights into rupture characteristics, and opens novel and promising avenues of future research.

## 1. Introduction

PyRadiomics [1], an automatic image processing tool that quantifies textural information from medical images, has been recently proposed for intracranial aneurysms morphological evaluation [2–6]. Radiomics, which allows for the evaluation of both shape morphology and intensity-based descriptors (histogram, texture and patterns), was previously used in medical research, particularly in oncology, for analysis of pathological imaging [7–12]. The process is based on the assumption that biomedical images contain disease-specific information that is not perceptible through visual inspection and traditional processing tools.

For cerebral aneurysm evaluation, radiomics use has been mostly restricted to morphological analysis [2–6] because of intensity homogeneity due to contrast enhanced catheter rotational angiography imaging, which renders texture evaluation less relevant for these volumes. However, research is emerging on use of radiomics texture and pattern analysis on angiographic aneurysmal data [13–15].

Cerebral aneurysms are degenerative processes resulting in pathological remodeling of the arterial wall based on the complex interaction between vessel wall biology and hemodynamic forces, which are considered a major contributor to aneurysm formation and rupture [16]. Among hemodynamic features, wall shear stress (WSS) and WSS derived features represent the focus of multiple studies which showed that WSS regulates the histological structure of arterial walls and is an important determinant of overall vascular structural remodeling [16]. Consequently, research was directed towards investigating variations in the distribution features of WSS between ruptured and unruptured aneurysms [17–20]. However, while research suggested strong associations

* Corresponding author at: Department of Neurosurgery, Tufts Medical Center, 800 Washington Street, Boston, MA 02111, USA.
*E-mail address:* Adel.Malek@tuftsmedicine.org (A.M. Malek).

https://doi.org/10.1016/j.jocn.2026.111851
Received 18 November 2025; Accepted 2 January 2026
Available online 7 January 2026
0967-5868/© 2026 Elsevier Ltd. All rights are reserved, including those for text and data mining, AI training, and similar technologies.

between WSS distribution parameters and rupture analysis, it resulted in conflicting findings regarding WSS, resulting in the high-versus-low WSS controversy [21] which remains to be resolved.

This study proposes an in-depth evaluation that goes beyond WSS distribution to evaluate WSS texture and patterns on the surface of intracranial aneurysms – a novel application of radiomics to the field of computational fluid dynamics (CFD). In addition, we propose a method for applying radiomics to transient CFD simulations, allowing for analysis of the WSS evolution over not only spatial but also temporal domains.

## 2. Materials and methods

### 2.1. Patient selection

A total of 75 catheter-based 3D rotational angiography datasets were included, representing patients with intracranial aneurysms, of which 33 had presented with rupture. For ruptured cases, imaging was acquired within the first 48 h to minimize the influence of vasospasm. Approval for this study was obtained from the Institutional Review Board ethics committee. Patient consent was waived because of the retrospective nature of the study not impacting patient clinical care.

### 2.2. Cerebral angiography and data processing

Three-dimensional catheter based cerebral angiograms were acquired using a calibrated biplane system. Data were reconstructed into 3D volumetric datasets using available clinical software. Volumes were processed for segmentation of aneurysm and surrounding vessels in 3D space using Amira visualization software version 5.3.3 (FEI, Hillsboro, OR) (Fig. 1). From each aneurysm, morphological features including maximum diameter (Dmax), maximum height (Hmax), height-to-width ratio (HW), aspect ratio (AR), size ratio (SR), and non-sphericity index (NSI) were computed as described in the literature [5].

Fluent meshing (Ansys 2021 R1, Ansys Inc., Lebanon, NH) was used to generate dynamic tetrahedral/prism meshes with boundary layer enhancement (Fig. 1A). To ensure fully laminar flow and prevent entrance effects, the segment proximal to the aneurysm was preserved to at least five times the parent vessel's diameter [17]. This enabled smooth, consistent flow pattern in the region of interest.

### 2.3. Computational fluid dynamics

Transient CFD simulations were performed using Ansys Fluent 2021 R1, modeling transient flow with a Carreau non-Newtonian profile to better approximation blood viscosity and dynamics [22]. Flow scaling factors were applied to ensure ideal parent vessel WSS conditions of approximately 1.5 Pa proximal to the aneurysm, accounting for variability in inflow vessel size, shape and length. Scaled pulsatile flow was applied at the inlet over three full cardiac cycles, with the third was used for analysis. Each cycle period was $T = 1$ sec with a time step of $t = 0.005$ sec, resulting in 200 time steps per cycle (peak-systole at $t = 0.16$ sec). Outlet gauge pressure was set to zero Pascal [23]. CFD solution data was exported during the 3rd cycle every 8th step, resulting in 25 time steps across entire cardiac cycle.

Post-processing analysis was performed using EnSight 2021 R1 (Ansys Inc., Lebanon, NH). The aneurysm dome was separated from surrounding vessels, and WSS values were exported at each time step as texture maps over aneurysm dome (Fig. 1B), resulting in 25 distinct 3D surface WSS per aneurysm.

### 2.4. Mapping 3D surface WSS to DICOM volume

For each time step, the exported WSS surface was translated to the coordinate origin, and each point projected onto the unit sphere, with the corresponding WSS value recorded on the sphere surface (Fig. 1C). The resulting unit sphere was projected on 2D using the UV mapping algorithm [24], a 3D modeling technique that enables texture mapping between 3D and 2D models. Fig. 2 illustrates WSS texture correspondence between unit sphere and the resulting 2D texture. Before grayscale DICOM conversion, WSS values were normalized over the entire cycle to a [0, 1] range, and logarithmic transformation was applied to enhance contrast at intensity extrema. Values were scaled by 1000 for conversion to DICOM image format. These 2D images representing spatial WSS on the aneurysm dome across time points, formed the input to radiomics as a 3D DICOM volume (Fig. 1D), capturing temporal WSS variations over the cardiac cycle.

### 2.5. Radiomics and feature extraction

The PyRadiomics package [1], a Python implementation, was used to extract radiomics features, which are organized into eight groups: 2D Shape Features, 3D Shape Features, First Order Features, Gray Level Co-occurrence Matrix Features, Gray Level Size Zone Matrix Features, Gray Level Run Length Matrix Features, Neighboring Gray Tone Difference Matrix Features, and Gray Level Dependence Matrix Features. This study focuses on histogram descriptors (first order) and gray level texture features. The complete list of radiomics features evaluated in this study is available as Supplemental Table 1. Details on Radiomics features descriptors available at **https://pyradiomics.readthedocs.io/en/latest/features.html**.

### 2.6. Statistical analysis

Statistical analysis was conducted using JMP Pro 17 (SAS Institute, Cary, NC) for morphological and radiomics features. Univariate comparisons were performed with Student's *t*-test, using a significance threshold of $p < 0.05$. For each feature, Receiver Operating Characteristic (ROC) curves were generated, and the area under the curve (AUC) was calculated to assess rupture status discrimination performance.

Multivariate logistic regression was performed using elastic net regularization to mitigate overfitting and address potential correlations among radiomics features. Separate analyses were conducted for morphological and radiomics parameters. Feature selection was integrated within the elastic net framework, using 5-fold cross-validation to promote model robustness and generalizability. Only features with non-zero coefficients were retained as predictive variables in the final model.

## 3. Results

### 3.1. Patient demographics

3D rotational angiographic datasets from 75 patients (61 females, 33 ruptured) harboring intracranial aneurysms were analyzed for the study. There was no statistically significant age difference between patients with ruptured vs. unruptured aneurysms ($61.96 \pm 10.85$ vs. $60.17 \pm 13.21$ years, $p = 0.53$).

### 3.2. Morphological feature analysis

Univariate statistical analysis of established size and shape descriptors revealed significantly higher values for ruptured aneurysms across all parameters. Maximum diameter (Dmax), maximum height (Hmax), Height/Width ratio, Aspect Ratio, Size Ratio, and the non-sphericity index (NSI) were significantly elevated in the ruptured group ($p < 0.05$ for all). AUC values ranged from 0.69 to 0.76, with the highest discrimination achieved by aspect ratio and size ratio (AUC = 0.76).

### 3.3. Radiomics analysis

Complete list of univariate analysis for all radiomics features

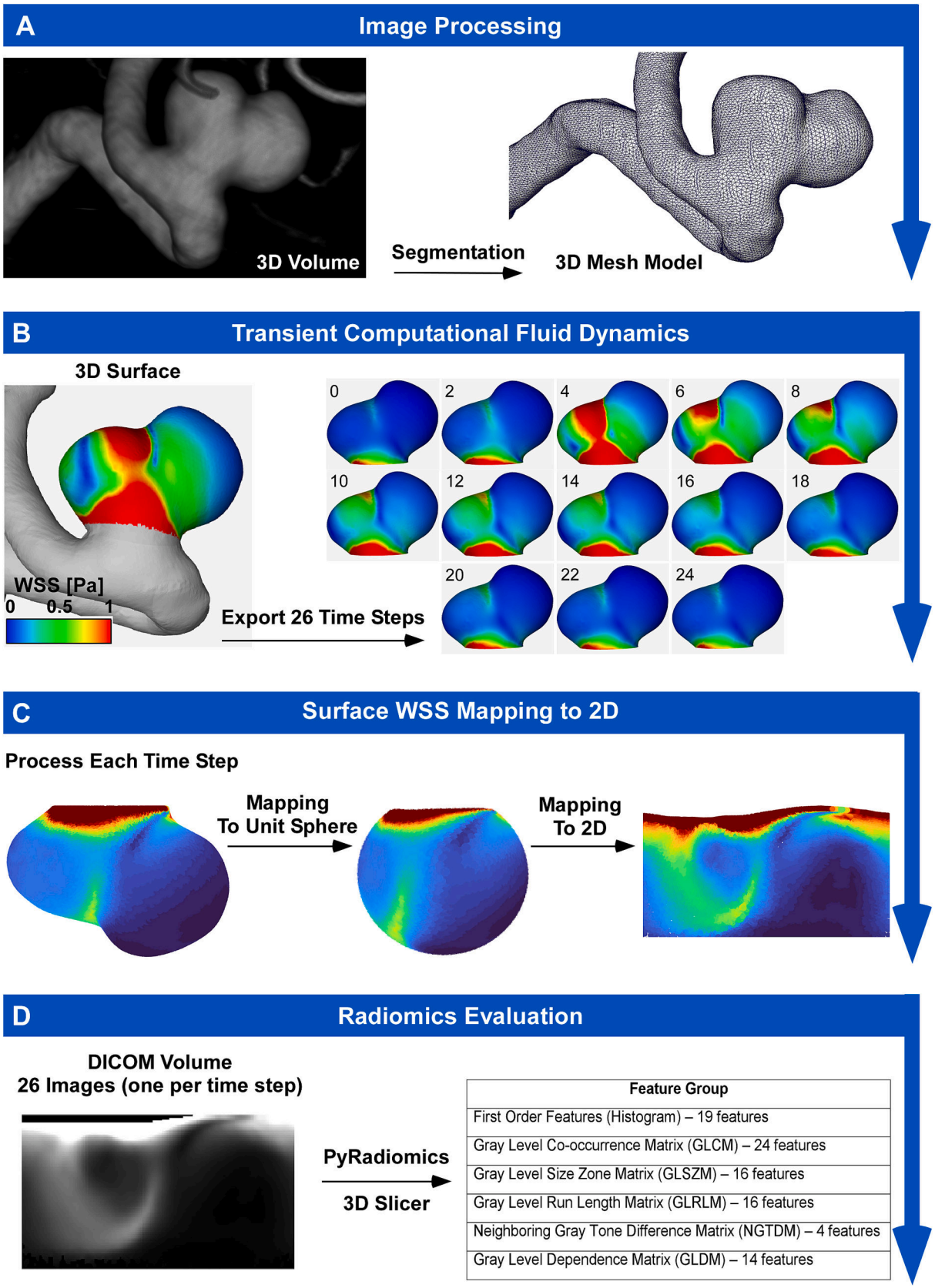



**Fig. 1.** radiomics of transient WSS processing steps. (A) 3D aneurysmal models are segmented from angiographic data. (B) Transient CFD simulations are performed and aneurysmal dome WSS is exported per time step (25 steps per cardiac cycle). (C) Surface WSS is projected to the unit sphere and mapped to 2D images. (D) The stack of 2D images representing WSS-derived texture maps for each time point, are saved as a DICOM volume. Radiomics features are generated, and features are evaluated as rupture status discriminants using univariate and multivariate statistical analysis.

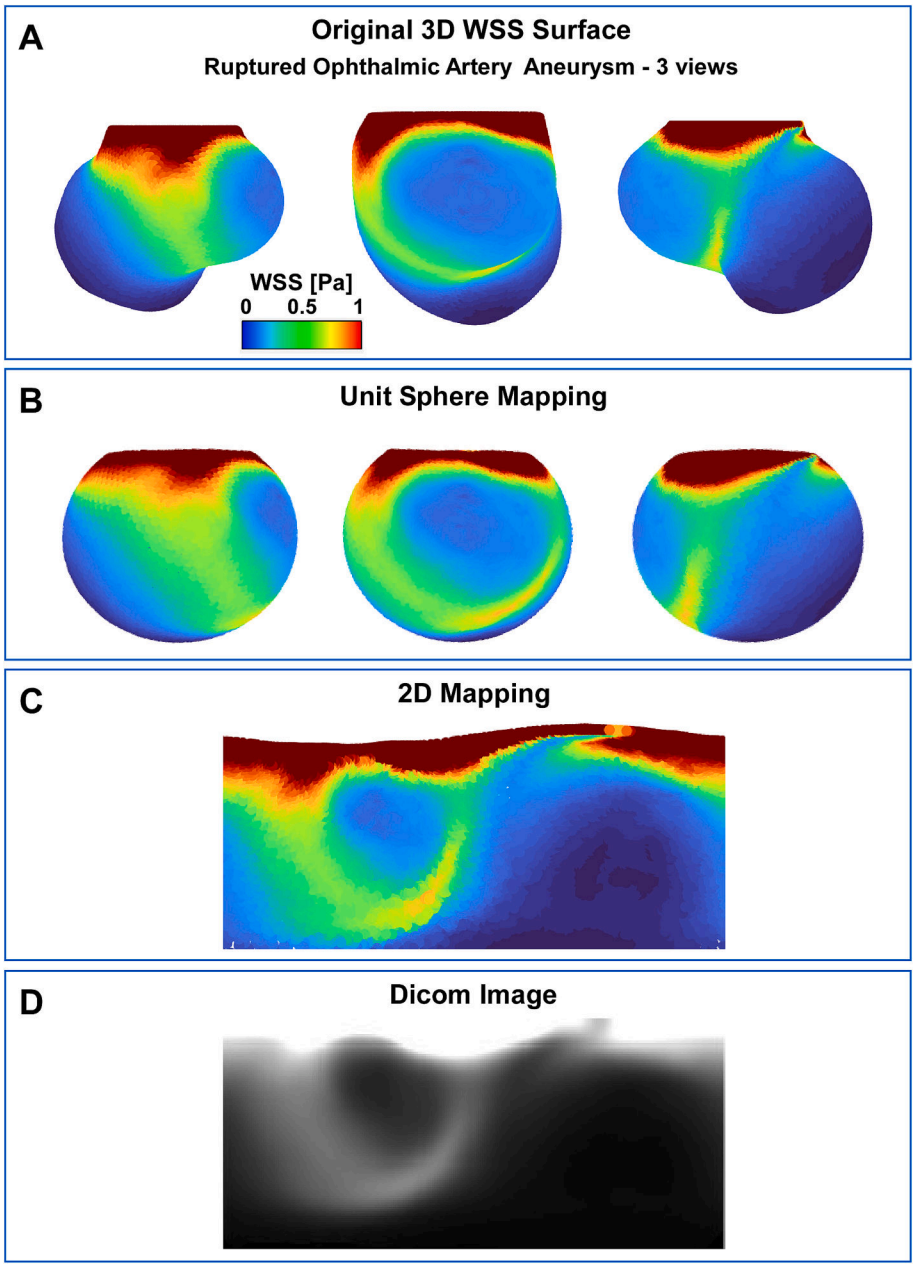



**Fig. 2.** (A) WSS values on the surface of a ruptured ophthalmic artery aneurysms shown from 3 distinct viewpoints. (B) Corresponding unit sphere mapping showing preservation of texture characteristics. (C) Projection of unit sphere to 2D plane using UV mapping algorithm. (D) 2D images are saved in a DICOM format for radiomics processing.

generated in this study is available as Supplemental Table 1. Univariate statistical analysis for selected features within each radiomics group is available in Table 1. Given the high dimensionality of radiomics feature sets, these results are presented as descriptive analysis, in order to illustrate general trends in spatial and temporal WSS-derived patterns and to inform subsequent multivariable modeling.

### 3.4. *First order features*

Ruptured aneurysms had negative WSS distribution skewness, whereas unruptured aneurysms had positive WSS distribution skewness ($p = 0.005$), suggesting a higher concentration of lower WSS values in the distribution of ruptured aneurysms. In addition, a trend was observed for ruptured aneurysms to have lower minimum WSS-derived intensity ($p = 0.05$) and a wider range of intensity values ($p = 0.05$).

### 3.5. *Gray level co-occurrence matrix features*

This group of features quantifies patterns based on frequency of specific combination of voxel occurrences within the image. Compared to unruptured, ruptured aneurysms are characterized by increased complexity and heterogeneity of WSS-derived intensity patterns. They have higher Difference Entropy (greater heterogeneity in magnitude and patterns, $p = 0.007$), higher Joint Average (distinct areas of high WSS-derived intensities, $p = 0.002$), higher Joint Entropy (increased variability and diversity of intensity patterns, $p = 0.02$), but lower Joint Energy (less texture homogeneity/uniformity, $p = 0.008$). In addition, ruptured aneurysms have significantly higher Sum Average ($p = 0.002$), which indicates occurrences of pairs of voxels with contrasting intensity values, suggesting a more diverse and complex texture pattern. Fig. 3 shows examples of ruptured and unruptured aneurysms with apparent differences in texture and patterns of WSS-derived images.

**Table 1**
WSS Normalized with Logarithmic Transformation. Radiomics analysis of transient wall shear stress data. Univariate statistical analysis of selected Radiomics descriptors for rupture status discrimination. Shown are mean and standard deviation. Statistical significance was assumed for $p < 0.05$. AUC represents the area under the ROC curve.

| Radiomics Descriptors | Ruptured | Unruptured | p Value | AUC |
|---|---|---|---|---|
| **FIRST ORDER FEATURES** | | | | |
| Minimum | −9302.5 ± 2037.6 | −8249.3 ± 2477.4 | 0.052 | 0.65 |
| Range | 9302.5 ± 2037.6 | 8249.3 ± 2477.4 | 0.052 | 0.65 |
| Skewness | −0.070214 ± 0.45537 | 0.21681 ± 0.39351 | 0.005 | 0.68 |
| **GRAY LEVEL CO-OCCURRENCE MATRIX** | | | | |
| DifferenceEntropy | 4.4629 ± 0.30317 | 4.2576 ± 0.32927 | 0.007 | 0.69 |
| JointAverage | 246.83 ± 75.157 | 191.17 ± 76.972 | 0.002 | 0.71 |
| JointEnergy | 0.0002197 ± 0.00011604 | 0.00032286 ± 0.00019256 | 0.008 | 0.66 |
| JointEntropy | 13.259 ± 0.69937 | 12.828 ± 0.84672 | 0.021 | 0.66 |
| SumAverage | 493.66 ± 150.31 | 382.34 ± 153.94 | 0.002 | 0.71 |
| **GRAY LEVEL SIZE ZONE MATRIX FEATURES** | | | | |
| ZonePercentage | 0.45762 ± 0.089714 | 0.40257 ± 0.1146 | 0.026 | 0.64 |
| ZoneVariance | 24.156 ± 32.999 | 46.826 ± 54.743 | 0.039 | 0.60 |
| SizeZoneNonUniformity | 33054 ± 11041 | 25107 ± 12761 | 0.006 | 0.68 |
| SizeZoneNonUniformityNormalized | 0.43098 ± 0.053554 | 0.38743 ± 0.068247 | 0.004 | 0.68 |
| LowGrayLevelZoneEmphasis | 0.000078473 ± 0.000054074 | 0.00012963 ± 0.000080637 | 0.003 | 0.71 |
| HighGrayLevelZoneEmphasis | 71745 ± 36542 | 49643 ± 37432 | 0.012 | 0.70 |
| SmallAreaHighGrayLevelEmphasis | 48068 ± 27295 | 33466 ± 27533 | 0.025 | 0.68 |
| SmallAreaLowGrayLevelEmphasis | 0.000050954 ± 0.000027934 | 0.000072052 ± 0.000040362 | 0.013 | 0.68 |
| **GRAY LEVEL RUN LENGTH MATRIX FEATURES** | | | | |
| RunPercentage | 0.94164 ± 0.015406 | 0.9303 ± 0.026022 | 0.030 | 0.63 |
| RunVariance | 0.12729 ± 0.054702 | 0.18313 ± 0.10095 | 0.005 | 0.65 |
| ShortRunHighGrayLevelEmphasis | 69755 ± 37860 | 46053 ± 37797 | 0.009 | 0.70 |
| ShortRunLowGrayLevelEmphasis | 0.000076672 ± 0.00006632 | 0.00013747 ± 0.00010421 | 0.005 | 0.71 |
| LongRunHighGrayLevelEmphasis | 90906 ± 48890 | 60793 ± 45692 | 0.008 | 0.70 |
| LongRunLowGrayLevelEmphasis | 0.00010848 ± 0.00010884 | 0.00022366 ± 0.00021267 | 0.006 | 0.72 |
| **NEIGHBOURING GRAY TONE DIFFERENCE MATRIX FEATURES** | | | | |
| Busyness | 0.021931 ± 0.016841 | 0.038479 ± 0.031909 | 0.009 | 0.69 |
| **GRAY LEVEL DEPENDENCE MATRIX FEATURES** | | | | |
| DependenceNonUniformity | 40466 ± 7447.2 | 34247 ± 10104 | 0.004 | 0.68 |
| HighGrayLevelEmphasis | 71745 ± 36542 | 49643 ± 37432 | 0.012 | 0.70 |
| LowGrayLevelEmphasis | 0.000081447 ± 0.000074349 | 0.00014974 ± 0.00012193 | 0.006 | 0.71 |

### 3.6. Gray level size zone matrix features

This group of features quantifies the size distribution of connected regions with specific WSS-derived intensities. Compared to unruptured, ruptured aneurysms are characterized by high Zone Percentage (high distribution of smaller connected regions, $p = 0.03$), but low Zone Variance (less variation in the size of distinct intensity clusters, $p = 0.04$). Together this suggests that ruptured aneurysms showcase a cluster distribution characterized by distinct WSS zones of relative similar sizes. In addition, ruptured aneurysms have a higher prevalence of clusters with high WSS-derived intensity (higher HighGrayLevelZoneEmphasis and lower LowGrayLevelZoneEmphasis) which tend to be smaller in size (higher SmallAreaHighGrayLevelEmphasis, $p = 0.025$).

### 3.7. Gray level run length matrix features

This group of features quantifies the distribution of intensity runs (consecutive voxels of same intensity) and captures information about the texture coarseness. Compared to unruptured, ruptured aneurysms are characterized by high Run Percentage (high percentage of sequential voxels, $p = 0.03$), but low Run Variance (reduced variability in the length of runs, $p = 0.005$). In addition, ruptured aneurysms have higher ShortRunHighGrayLevelEmphasis ($p = 0.009$) and LongRunHighGrayLevelEmphasis ($p = 0.008$) (high distribution of short and long runs of high WSS-derived values, respectively) with low ShortRunLowGrayLevelEmphasis ($p = 0.005$) and LongRunLowGrayLevelEmphasis ($p = 0.006$). Together these findings suggest that ruptured aneurysms are characterized by the presence of short and long runs of high WSS values which are clustered together (low Run Variance) and not dispersed in the spatial and temporal domain.

### 3.8. Neighboring gray tone difference matrix features

This group of features quantifies differences in gray tone values between neighboring voxels in the image. Only Busyness was statistically significant in this group, with ruptured aneurysms exhibiting lower Busyness compared to unruptured, suggesting gradual changes in intensity, with high and low WSS-derived intensities cluster together, respectively, rather than disperse, as implied by higher JointAverage.

### 3.9. Gray level dependence matrix features

Features in this group quantify voxel intensity dependencies in an image within a particular size neighborhood. Ruptured aneurysms exhibit significantly higher DependenceNonUniformity ($p = 0.004$) indicating heterogeneity among dependencies in the image, reflecting presence of distinct regions with different voxel dependencies. HighGrayLevelEmphasis ($p = 0.01$), and SmallDependenceHighGrayLevelEmphasis ($p = 0.03$) were significantly higher in the ruptured group compared to unruptured, whereas LowGrayLevelEmphasis ($p = 0.006$), and SmallDependenceLowGrayLevelEmphasis ($p = 0.01$) were significantly lower,

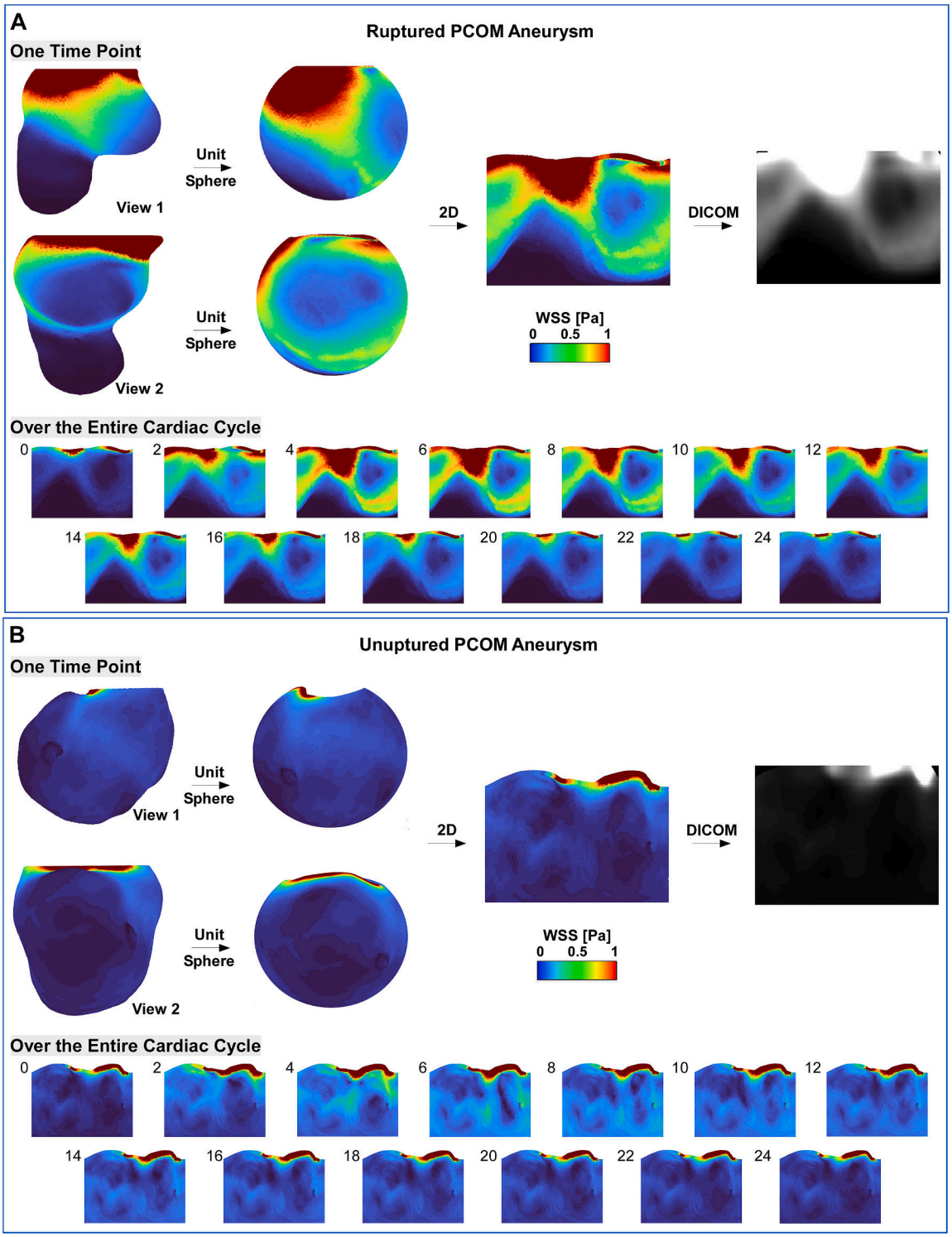



**Fig. 3.** (A) Example of the processing pipeline on a ruptured posterior communicating aneurysm. Detail of mapping from 3D WSS to a DICOM image for one time step. Series of 2D planar projections of the WSS over the entire cardiac cycle. The numbers represent time steps. (B) Example of the processing pipeline on an unruptured posterior communicating aneurysm. Detail of mapping from 3D WSS to a DICOM image for one time step. Series of 2D planar projections of the WSS over the entire cardiac cycle. The numbers represent time steps.

indicating a higher distribution of small-scale dependencies involving high WSS values.

### 3.10. Multivariate analysis

Elastic net regression with 5-fold cross-validation identified four WSS radiomics features as independent predictors of rupture status: RunLengthNonUniformity, Zone Entropy, 90Percentile, and Cluster Shade. Among these, RunLengthNonUniformity (estimate: +6.70) and 90Percentile (estimate: +2.50) had positive coefficients, suggesting that higher texture non-uniformity and higher local WSS-derived intensity values are associated with increased rupture risk. In contrast, Zone

Entropy (estimate: −1.52) and Cluster Shade (estimate: −0.42) had negative coefficients, indicating that lower entropy and reduced asymmetry in WSS intensity distribution are linked to rupture in the presence of the other selected features.

The combined multivariate model achieved an AUC of 0.81, with sensitivity of 0.82 and specificity of 0.72. In comparison, the multivariate morphological model achieved an AUC of 0.76, with sensitivity of 0.79 and specificity of 0.67.

## 4. Discussion

Radiomics, a comprehensive approach for evaluating various aspects of medical imaging data, provides several advantages in the evaluation of volumetric images, including the automatic and reproducible assessment of morphological and texture characteristics. In the context of aneurysm evaluation, morphological 2D and 3D radiomics features have previously been proposed as discriminators of rupture status [2–6], and their comparative value compared to established shape descriptors has been discussed [3]. The utilization of texture and pattern radiomics features for aneurysmal imaging is a relatively new area of research that is currently emerging in the literature. Radiomics descriptors have been utilized for pattern analysis on magnetic resonance angiographic aneurysmal data [13], to analyze angiographic parametric imaging and serve as biomarkers for assessing blood flow contrast within the aneurysmal sac [14], and to predict the occlusion of aneurysms before and after intervention, offering valuable insights into the treatment outcomes [15].

In addition to morphological evaluation of aneurysmal shapes, CFD simulations are used to provide insight into the mechanisms of aneurysm rupture, with many studies focusing on WSS [17–20], as an important contributor to aneurysmal origination and possible rupture [16].

Recently, radiomics has also been applied to volumetric CFD-derived velocity fields, demonstrating that histogram and texture descriptors of intra-dome flow patterns can discriminate aneurysm rupture status [25]. This present study extends the use of radiomics to surface-based CFD fields, applying it to transient WSS data and evaluating not only first-order statistics but also spatial and temporal texture patterns that evolve during the cardiac cycle. Following CFD simulations, WSS distributions were exported for consecutive time points. 3D surface WSS were mapped to 2D by projection to unit sphere, followed by normalization and logarithmic transformation of data for detailed evaluation at extrema. 2D images representing consecutive time points, formed the input to radiomics as 3D DICOM volumes. Imaging volumes corresponding to the WSS evolution over an entire cardiac cycle were analyzed using PyRadiomics, allowing for evaluation not only in the spatial (aneurysm dome), but also in the temporal domain (multiple time points of the cardiac cycle). To our knowledge, this is the first study to apply radiomics analysis to transient CFD-derived wall shear stress distributions on aneurysm surfaces.

The analysis of radiomics features in ruptured vs. unruptured aneurysms revealed distinct patterns and texture characteristics. Ruptured aneurysms exhibit increased complexity and heterogeneity in the intensity patterns derived from WSS. This is evident through higher Difference Entropy, Joint Average, and Joint Entropy, indicating greater variability, diversity, and distinct areas of high WSS-derived intensities. Additionally, ruptured aneurysms display higher Sum Average, suggesting the occurrence of contrasting intensity values and a more diverse and complex texture pattern. The cluster distribution in ruptured aneurysms is characterized by high Zone Percentage but low Zone Variance, indicating the presence of distinct WSS zones of relatively similar sizes. Furthermore, ruptured aneurysms also exhibit a higher percentage of sequential voxels (Run Percentage) but reduced variability in the length of runs (Run Variance). Moreover, the presence of short and long runs of high WSS values clustered together is highlighted by higher ShortRunHighGrayLevelEmphasis and LongRunHighGrayLevelEmphasis, while lower ShortRunLowGrayLevelEmphasis and LongRunLowGrayLevelEmphasis indicate a lower distribution of low WSS values. The higher DependenceNonUniformity observed in ruptured aneurysms reflects heterogeneity in voxel dependencies and the presence of distinct regions with different dependencies. Collectively, these findings suggest unique radiomics signatures associated with ruptured aneurysms, providing valuable insights into hemodynamic characteristics of aneurysmal rupture. Multivariate analysis for rupture status discrimination resulted in an area under the curve (AUC) value of 0.81 (sensitivity 0.82, specificity 0.72).

The innovative utilization of radiomics in the evaluation of transient CFD data opens exciting opportunities for future research, offering a novel perspective on the understanding of aneurysmal rupture. Radiomics analysis as presented here can provide valuable insights that might otherwise go unnoticed using traditional processing tools. Importantly, this methodology can be extended to any transient surface field generated by CFD (such as pressure, oscillatory shear index, etc.) providing a framework for analyzing complex spatial and temporal data. The incorporation of radiomics in CFD evaluation not only enhances our understanding of aneurysmal rupture, but also paves the way for further exploration and advancement in this important area of research.

### 4.1. Study limitations

The current study is a retrospective analysis aimed at classifying the rupture status of aneurysms. It does not serve as a predictive tool for aneurysmal rupture, but rather aims to identify features that can differentiate between aneurysms that have already ruptured and those that have not. This is a limitation we share with many previous studies relevant to our research. The retrospective nature of the study assumes that the surface of the aneurysms do not significantly change following rupture. While prior evidence suggests that such changes are unlikely [26], additional conclusive data on this topic is still needed.

A further consideration is that radiomics analysis generates a large number of quantitative features, therefore research must address challenges associated with high-dimensional feature spaces, including multiple hypothesis testing, feature collinearity, and the risk of model overfitting [27]. While our multivariable analysis explicitly mitigates these concerns through the use of elastic net regularization, the univariate radiomics analysis presented in this study is intended as an exploratory statistical screening. Given the dimensionality of radiomics feature sets, these analyses were used to characterize general trends across feature groups and to provide intuitive context for the subsequent multivariable modeling.

It should be noted that while our methodology aligns with several best-practice elements outlined in the Radiomics Quality Score (RQS) [28,29], including detailed reporting of preprocessing steps, use of the open-source PyRadiomics framework, appropriate feature reduction and overfitting control through elastic net regularization with cross-validation, it also has some limitations, such as its retrospective design and the absence of external validation.

These limitations are expected for a proof-of-concept study aimed at establishing feasibility and testing the underlying principles of a novel radiomics methodology. Importantly, this work represents the first application of radiomics to transient CFD-derived wall shear stress fields, incorporating both spatial and temporal texture information; as such, the biological and hemodynamic interpretation of individual radiomics features remains preliminary and hypothesis-generating and will require further investigation in future validation-focused studies. Ultimately, the potential of these features to serve as predictive markers can only be confirmed through further validation and prospective studies that evaluate their clinical relevance and practical application in assessing intracranial aneurysms.

## 5. Conclusion

We propose a novel approach to CFD evaluation of intracranial aneurysms, which extends the use of radiomics beyond angiographic

analysis and allows for the evaluation of WSS temporal evolution over an entire cardiac cycle, not only in terms of distribution, but also texture and imaging patterns. Our radiomics analysis of WSS-derived images showed that ruptured aneurysms are characterized by increased complexity and heterogeneity, with distinct regions of low and high WSS intensities. Multivariate analysis for rupture status discrimination resulted in an area under the curve (AUC) value of 0.81 (sensitivity 0.82, specificity 0.72). Importantly, this methodology can be extended to any transient surface field generated by CFD providing a generalizable framework for analyzing complex spatial and temporal data. It provides valuable insights that may be overlooked by conventional processing tools and opens promising avenues of future research and possible applications of radiomics concepts to aneurysm evaluation.

## 6. Contributorship Statement

All authors are justifiably credited with authorship according to the authorship criteria. In detail: AL acquisition of data, image processing, analysis and interpretation of data, drafting of the manuscript; AMM conception, design, acquisition of data, analysis and interpretation of data, critical revision, final approval.

## 7. IRB approval

This research was approved by Tufts Health Sciences Campus Institutional Review Board (IRB# 9035). Patient consent was waived because of the retrospective nature of the study not impacting patient clinical care.

## 8. Sources of Support

None.

This research was approved by Tufts Health Sciences Campus Institutional Review Board (IRB# 9035). All procedures were performed in compliance with relevant laws and institutional guidelines and have been approved by the appropriate institutional committee. Patient consent was waived because of the retrospective nature of the study not impacting patient clinical care.

## CRediT authorship contribution statement

**Alexandra Lauric:** Writing – original draft, Visualization, Methodology, Investigation, Formal analysis, Data curation. **Adel M. Malek:** Writing – review & editing, Supervision, Resources, Project administration, Data curation, Conceptualization.

## Declaration of competing interest

The authors declare that they have no known competing financial interests or personal relationships that could have appeared to influence the work reported in this paper.

## Appendix A. Supplementary data

Supplementary data to this article can be found online at https://doi.org/10.1016/j.jocn.2026.111851.

## References

[1] van Griethuysen JJM, Fedorov A, Parmar C, Hosny A, Aucoin N, Narayan V, et al. Computational Radiomics System to Decode the Radiographic Phenotype. Cancer Res 2017;77:e104–7.
[2] Zhang Y, Ma C, Liang S, Yan P, Liang F, Guo F, et al. Morphologic Feature Elongation can Predict Occlusion Status following Pipeline Embolization of Intracranial Aneurysms. World Neurosurg 2018;119:e934–40.
[3] Ludwig CG, Lauric A, Malek JA, Mulligan R, Malek AM. Performance of Radiomics derived morphological features for prediction of aneurysm rupture status. Journal of neurointerventional surgery 2020.
[4] Liu Q, Jiang P, Jiang Y, Ge H, Li S, Jin H, et al. Prediction of Aneurysm Stability using a Machine Learning Model based on PyRadiomics-Derived Morphological Features. Stroke 2019;50:2314–21.
[5] Lauric A, Ludwig CG, Malek AM. Enhanced Radiomics for Prediction of Rupture Status in Cerebral Aneurysms. World Neurosurg 2022;159:e8–22.
[6] Chen G, Lu M, Shi Z, Xia S, Ren Y, Liu Z, et al. Development and validation of machine learning prediction model based on computed tomography angiography–derived hemodynamics for rupture status of intracranial aneurysms: a chinese multicenter study. Eur Radiol 2020;30:5170–82.
[7] Hyun SH, Ahn MS, Koh YW, Lee SJ. A Machine-Learning Approach using PET-Based Radiomics to Predict the Histological Subtypes of Lung Cancer. Clin Nucl Med 2019.
[8] Wang K, Lu X, Zhou H, Gao Y, Zheng J, Tong M, et al. Deep learning Radiomics of shear wave elastography significantly improved diagnostic performance for assessing liver fibrosis in chronic hepatitis B: a prospective multicentre study. Gut 2019;68:729–41.
[9] Toivonen J, Montoya Perez I, Movahedi P, Merisaari H, Pesola M, Taimen P, et al. Radiomics and machine learning of multisequence multiparametric prostate MRI: Towards improved non-invasive prostate cancer characterization. PLoS One 2019;14:e0217702.
[10] Fan Y, Chen C, Zhao F, Tian Z, Wang J, Ma X, et al. Radiomics-based Machine Learning Technology Enables Better Differentiation between Glioblastoma and Anaplastic Oligodendroglioma. Front Oncol 2019;9:1164.
[11] Chen C, Ou X, Wang J, Guo W, Ma X. Radiomics-based Machine Learning in Differentiation between Glioblastoma and Metastatic Brain Tumors. Front Oncol 2019;9:806.
[12] Zhou Z, Chen L, Sher D, Zhang Q, Shah J, Pham NL, et al. Predicting Lymph Node Metastasis in Head and Neck Cancer by Combining Many-objective Radiomics and 3-dimensioal Convolutional Neural Network through Evidential reasoning. Conference proceedings : Annual International Conference of the IEEE Engineering in Medicine and Biology Society IEEE Engineering in Medicine and Biology Society Annual Conference 2018;2018:1–4.
[13] Yamanouchi M, Arimura H, Kodama T, Urakami A. Prediction of Intracranial Aneurysm Rupture Risk using Non-Invasive Radiomics Analysis based on Follow-up magnetic Resonance Angiography Images: a Preliminary Study. Appl Sci 2022;12:8615.
[14] Podgorsak AR, Rava RA, Shiraz Bhurwani MM, Chandra AR, Davies JM, Siddiqui AH, et al. Automatic radiomic feature extraction using deep learning for angiographic parametric imaging of intracranial aneurysms. Journal of neurointerventional surgery 2020;12:417–21.
[15] Shiraz Bhurwani MM, Waqas M, Podgorsak AR, Williams KA, Davies JM, Snyder K, et al. Feasibility study for use of angiographic parametric imaging and deep neural networks for intracranial aneurysm occlusion prediction. Journal of neurointerventional surgery 2020;12:714–9.
[16] Sforza DM, Putman CM, Cebral JR. Hemodynamics of Cerebral Aneurysms. Annu Rev Fluid Mech 2009;41:91–107.
[17] Lauric A, Hippelheuser J, Cohen AD, Kadasi LM, Malek AM. Wall shear stress association with rupture status in volume matched sidewall aneurysms. Journal of neurointerventional surgery 2014;6:466–73.
[18] Salimi Ashkezari SF, Mut F, Chung BJ, Yu AK, Stapleton CJ, See AP, et al. Hemodynamics in aneurysm blebs with different wall characteristics. Journal of neurointerventional surgery 2020. neurintsurg -2020-016601.
[19] Suzuki T, Stapleton CJ, Koch MJ, Tanaka K, Fujimura S, Suzuki T, et al. Decreased wall shear stress at high-pressure areas predicts the rupture point in ruptured intracranial aneurysms. J Neurosurg 2020;132:1116–22.
[20] Axier A, Rexiati N, Wang Z, Cheng X, Su R, Aikeremu R, et al. Effect of hemodynamic changes on the risk of intracranial aneurysm rupture: a systematic review and meta-analysis. Am J Transl Res 2022;14:4638–47.
[21] Meng H, Tutino VM, Xiang J, Siddiqui A. High WSS or Low WSS? complex Interactions of Hemodynamics with Intracranial Aneurysm Initiation, growth, and Rupture: Toward a Unifying Hypothesis. AJNR Am J Neuroradiol 2013.
[22] Schirmer CM, Malek AM. Wall shear stress gradient analysis within an idealized stenosis using non-Newtonian flow. Neurosurgery. 2007;61:853-63; discussion 63-4.
[23] Bowker TJ, Watton PN, Summers PE, Byrne JV, Ventikos Y. Rest versus exercise hemodynamics for middle cerebral artery aneurysms: a computational study. AJNR Am J Neuroradiol 2010;31:317–23.
[24] Mullen T. Mastering blender: John Wiley & Sons; 2011.
[25] Lauric A, Malek AM. A Novel Application of Radiomics Analysis for Computational Fluid Dynamics Evaluation of Cerebral Aneurysms. World Neurosurg 2026;205:124602.
[26] Asari S, Ohmoto T. Natural history and risk factors of unruptured cerebral aneurysms. Clin Neurol Neurosurg 1993;95:205–14.
[27] Rizzo S, Botta F, Raimondi S, Origgi D, Fanciullo C, Morganti AG, et al. Radiomics: the facts and the challenges of image analysis. Eur Radio Exp 2018;2:36.
[28] Barry N, Kendrick J, Molin K, Li S, Rowshanfarzad P, Hassan GM, et al. Evaluating the impact of the Radiomics Quality score: a systematic review and meta-analysis. Eur Radiol 2025;35:1701–13.
[29] Lambin P, Leijenaar RTH, Deist TM, Peerlings J, de Jong EEC, van Timmeren J, et al. Radiomics: the bridge between medical imaging and personalized medicine. Nat Rev Clin Oncol 2017;14:749–62.